Research Square

Preprints are preliminary reports that have not undergone peer review.
They should not be considered conclusive, used to inform clinical practice,
or referenced by the media as validated information.

Multiepitope mRNA vaccine against Fasciola hepatica confers T-cell- mediated protection in mice

Javier Sánchez-Montejo
University of Salamanca
Cristina Teodosio
Instituto de Investigación Biomédica de Salamanca
Julio López-Abán
University of Salamanca
Raúl Manzano-Román
University of Salamanca
Julio Pozo
Cytognos SL/ Water Biosciences
María Ángeles Solinís
University of the Basque Country
Ana del Pozo-Rodríguez
University of the Basque Country
Tania Strilets
University of Virginia
Mariano García-Blanco
University of Virginia
Belén Vicente
belvi25@usal.es
University of Salamanca
Antonio Muro
University of Salamanca

Article

Keywords:

Posted Date: April 30th, 2026

DOI: https://doi.org/10.21203/rs.3.rs-9441135/v1

License: This work is licensed under a Creative Commons Attribution 4.0 International License.
Read Full License

Additional Declarations: Competing interest reported. JP is an employee of Cytognos/Water Biosciences (formerly BD Biosciences), Salamanca, and declares no non-financial competing interests. MG-B is cofounder and has a significant equity stake in Circurna, Inc, which is commercializing RNA-based vaccines and therapies, and declares no non-financial competing interests. All other authors declare no financial or non-financial competing interests

Abstract

Fasciolosis is a zoonotic disease causing morbidity in humans and economic losses in livestock, with no vaccine available. Messenger RNA vaccines have advantages over classical vaccination strategies, but have not been tested for protection against *Fasciola hepatica*. We designed an mRNA construct encoding three MHC class II T-cell epitopes fused to eGFP, and formulated it into solid lipid nanoparticles. BALB/c mice received a prime-boost immunization before oral challenge with *F. hepatica* metacercariae. The construct eGFP-Fh3Tq drove the expansion of terminally differentiated effector memory $CD4^+$ and $CD8^+$ T cells, with no B-cell expansion. Furthermore, after restimulation with the peptide, splenocytes showed a Th1 and Th17-skewed cytokine profile. Upon challenge, vaccination with the eGFP-Fh3Tq RNA led to a 71% reduction in mean worm burden, significantly lower number of hepatic lesions, and a 67% survival *vs.* 0% in the unvaccinated control group. This is the first demonstration that an mRNA vaccine encoding defined T-cell epitopes of *F. hepatica* confers protection *in vivo*.

Introduction

Fasciolosis is a zoonotic disease caused by the liver fluke *Fasciola hepatica*, a foodborne trematode that infects a broad spectrum of mammalian hosts, including humans and grazing livestock [1]. The World Health Organization classifies fasciolosis as a neglected tropical disease, with an estimated 2.4 million people infected and over 180 million at risk globally [2]. In livestock, it results in annual economic losses exceeding 3 billion US dollars worldwide due to decreased milk and meat production, impaired fertility, and treatment expenses [3]. Current control strategies depend primarily on triclabendazole, the only drug effective against both juvenile and adult parasite stages; however, the emergence of triclabendazole-resistant strains in several countries poses significant challenges for future disease management [4,5].

During the past three decades, a variety of antigens have been investigated as vaccine candidates against *F. hepatica*, including fatty acid-binding proteins, cathepsin proteases, glutathione S-transferases, leucine aminopeptidases, peroxiredoxins, and helminth defense molecules (HDMs) [6]. Although some candidates have demonstrated partial protection in animal models, typically reducing worm burden by 40–70%, none have achieved complete protection, and no commercial vaccine is currently licensed for either animal or human fasciolosis [7].

Peptide vaccines use small fragments of immunologically relevant proteins with favorable safety profiles [8]. Early work by Muro et al. (2007) identified two T-cell epitopes from the *F. hepatica* fatty acid-binding protein Fh15 and demonstrated that these epitopes conferred partial protection in rabbits and enhanced survival in mice [9]. This provided the first evidence that defined T-cell epitopes from *F. hepatica* antigens could induce protective immunity. Rojas-Caraballo et al. (2014) subsequently expanded this approach by using bioinformatic prediction to identify B- and T-cell epitopes from multiple parasite proteins, showing that synthetic peptide cocktails could confer partial protection in mice [10]. Building on these findings, a

genome-wide screen of *F. hepatica* identified 55 MHC class II-binding peptide candidates with high immunogenic potential [11].

Messenger RNA (mRNA) vaccines are a promising platform for delivering these epitopes that could be used against parasites. When translated within host cells, mRNA-encoded antigens are processed endogenously and can be presented via both MHC class I and class II pathways [12]. In addition to efficient antigen presentation, mRNA vaccines offer scalability, rapid design iteration, and the capacity to encode multiple antigens within a single construct [13]. Although mRNA vaccines have significantly advanced the prevention of infectious diseases since the COVID-19 pandemic, their use against parasitic infections remains in the early stages. Recent studies by Oliveira et al. (2025) demonstrated that mRNA constructs encoding *Schistosoma mansoni* tetraspanin-2 (Sm-TSP-2), formulated in lipid nanoparticles (LNPs), reduced worm and egg burdens by up to 67% in mice [14]. Similarly, mRNA vaccine candidates for hookworm [15], as well as mRNA approaches targeting *Toxoplasma gondii* [16] and *Plasmodium vivax* [17], have yielded encouraging results. A full-length FABP (Fh15) mRNA-LNP vaccine has been developed and shown to elicit robust innate, cellular, and humoral immune responses against *F. hepatica* antigens in mice [18]. However, to date, no mRNA vaccine against *F. hepatica* has been evaluated in an *in vivo* protection model.

In this study, an eGFP-fused multi-epitope mRNA construct was formulated in solid lipid nanoparticles (SLN), and its immunogenicity and protective efficacy were evaluated in a murine model of *F. hepatica* infection. For the first time, a multiepitope mRNA vaccine reduced the parasitic burden and improved the survival of *F. hepatica* infected mice

Materials and methods

mRNA preparation

Sequences of the epitopes T14, T15, and T16 used by Rojas-Caraballo *et al., (2014)* [10] were cloned downstream of the eGFP coding sequence, spaced by GPGPG linkers, in the expression vector described in [11], and the mRNA was prepared as previously described therein. Briefly, the plasmid containing the expression cassette was linearized overnight with BspQI (R0712S, NEB, Ipswich, MA, USA) and purified by phenol-chloroform extraction. Subsequently, 1 µg of linearized plasmid was used as template for overnight *in vitro* transcription (IVT) at 37°C (HiScribe® T7 Quick High Yield RNA Synthesis Kit, E2050S, NEB, Ipswich, MA, USA) with co-transcriptional capping using 4 mM CleanCap AG (TriLink Biotechnologies, San Diego, CA, USA). The resulting mRNA was treated with DNase I (M0303, NEB, Ipswich, MA, USA) to remove the DNA template, then precipitated by adding LiCl to a final concentration of 2.5 M. The mixture was incubated for 1 hour at − 20°C and centrifuged for 30 minutes at maximum speed. The pellet was washed twice with 70% ethanol, resuspended in nuclease-free water, and quantified by A260/A280 spectrophotometry using a NanoDrop 2000 (Thermo Scientific, Waltham, MA, USA). Double-stranded RNA (dsRNA) contaminants were subsequently removed by cellulose

chromatography as described by [19]. Briefly, 500 µg of mRNA in chromatography buffer (10 mM HEPES, 0.1 mM EDTA, 125 mM NaCl, and 16% ethanol) was loaded onto a NucleoSpin filter column (740606, Macherey-Nagel) pre-packed with 0.14 g of cellulose (C6288, Sigma-Aldrich). The column was agitated for 30 minutes and then centrifuged at 14,000 × g for 60 seconds to collect the eluate. The eluate was precipitated with 0.1 volumes of 3 M sodium acetate and 1 volume of isopropanol, washed with 70% ethanol, and resuspended in nuclease-free water. mRNA integrity was assessed by electrophoresis on a 1% agarose gel in TAE buffer with ethidium bromide staining.

In vitro testing and Western blot

Protein expression from the mRNA constructs was verified by transfecting HEK293T cells with Lipofectamine MessengerMAX (LMRNA003, Invitrogen, Waltham, MA, USA). Cells seeded in 24-well plates at approximately 70% confluence were transfected with 2.5 or 5 µg of purified mRNA using 1 µL of MessengerMAX per well according to the manufacturer's instructions and incubated for 24 h. Cells were then photographed using an EVOS FLoid (Thermo Scientific), and lysed in 1× RIPA buffer (9806S, Cell Signaling Technologies, Danvers, MA, USA) supplemented with protease inhibitors (5871, Cell Signaling Technologies). Lysates were clarified by centrifugation at maximum speed for 10 min, and total protein concentration in the supernatant was determined using the Pierce BCA protein assay kit (23225, Thermo Scientific, Waltham, MA, USA). Samples were denatured at 95°C for 10 min in 1× SDS-PAGE loading buffer (MB11701, NZYTech, Lisbon, Portugal) containing β-mercaptoethanol. Thirty micrograms of total protein per sample were resolved by SDS-PAGE on precast gradient gels (MB46601, NZYTech) and transferred onto nitrocellulose membranes (88018, Thermo Scientific). Membranes were blocked for 60 min with 5% skimmed milk and then incubated overnight at 4°C with an anti-His tag antibody (MA121315, Invitrogen) diluted 1:1,000 in 5% skimmed milk. After three washes of 10 min each in 1× PBS containing 0.1% Tween-20, membranes were incubated for 60 min with an anti-mouse IgG-HRP secondary antibody (A9044, Sigma-Aldrich, St. Louis, MO, USA) diluted 1:10,000 in 5% skimmed milk. Following three additional 10-min washes in 1× PBS 0.1% Tween-20, signal was detected by incubation with NZY Advanced ECL substrate (MB40201, NZYTech) for 3 min, and images were acquired on a ChemiDoc system (Bio-Rad, Hercules, CA, USA). Transfection efficiency at single cell level (frequency and level of expression) were evaluated by flow cytometry, employing a five laser Aurora spectral flow cytometer (Cytek Biosciences, Fremont, CA). Positive events were identified by gating against negative cells, using a 99.9th percentile threshold.

Solid lipid nanoparticle preparation

Solid lipid nanoparticles (SLN) were prepared by the solvent emulsification-evaporation technique as previously described [20]. Briefly, Precirol® ATO 5 (glyceryl palmitostearate; kindly provided by Gattefossé, Madrid, Spain) was dissolved in dichloromethane at 5% (w/v) and mixed with an aqueous phase containing 1,2-dioleoyl-3-trimethylammonium-propane chloride salt (DOTAP, 0.4% w/v; Avanti Polar

Lipids, Alabaster, AL, USA) and Tween 80 (0.1% w/v; Panreac, Madrid, Spain). The mixture was sonicated for 30 s, and the organic solvent was evaporated.

To assemble the mRNA delivery vectors, *in vitro*-transcribed mRNA was first complexed with protamine sulfate (Grade X, from salmon; Sigma-Aldrich, Madrid, Spain) in aqueous solution for 5 min. An aqueous solution of hyaluronic acid (HA; Mw 100 kDa; Lifecore Biomedical, Chaska, MN, USA) was then added and allowed to interact for 15 min. Finally, the SLN suspension was incorporated into the mRNA-protamine-HA complexes. The final vectors were formed through electrostatic interactions among all components at a weight ratio of HA:protamine:mRNA:SLN = 0.5:0.5:1:5.

Solid lipid nanoparticle characterization

The mean size and polydispersity index (PDI) of SLN and mRNA vectors were measured by dynamic light scattering (DLS), and the ζ-potential was determined by laser Doppler velocimetry, using a Zetasizer Nano ZS (Malvern Instruments, Worcestershire, UK). Samples were diluted in Milli-Q water prior to measurement.

The capacity of the SLN-based vectors to bind and release the mRNA cargo was evaluated by agarose gel electrophoresis (1.2% agarose, stained with GelRed™; Biotium, Fremont, CA, USA). Vectors were diluted in Milli-Q water to a final concentration of 0.12 µg mRNA/µL. For release assays, diluted vectors were incubated with sodium dodecyl sulfate (SDS; Sigma-Aldrich) at a final concentration of 1% at room temperature to test the ability of the formulations to release the nucleic acid. A RiboRuler High Range RNA Ladder (Thermo Fisher Scientific, Madrid, Spain) was included as a molecular-weight reference, and naked mRNA as an integrity control. Gels were run at 75 V for 60 min and visualized using a Uvitec Uvidoc D-55-LCD-20M Auto transilluminator (Cambridge, UK).

The fraction of mRNA exposed on the surface of the nanoparticle vectors was quantified using the Quant-iT™ RiboGreen RNA Assay Kit (Thermo Fisher Scientific, Madrid, Spain), which employs a fluorescent dye that becomes intensely fluorescent upon binding accessible RNA [21]. A calibration curve was prepared according to the manufacturer's instructions. Vectors were diluted in 1× TE buffer, incubated with the working reagent for 5 min, and fluorescence was measured at λ ~ ex~/λ ~ em ~ = 480/530 nm using a GloMax®-Multi Detection System microplate reader (Promega, Madison, WI, USA).

Animal handling and experimental design

Animal procedures were conducted in accordance with Spanish (RD 53/2013) and European Union (Directive 2010/63/CE) regulations on animal experimentation. The accredited Animal Experimentation Facilities (Registration number: PAE/SA/001) of the University of Salamanca (USAL) were used for such procedures. Animals were maintained in standard polycarbonate and wire cages, with controlled 12-hour light and dark periods, a temperature of 23–25°C, and food and water available *ad libitum*. The USAL's

Research Ethics Committee approved the procedures used in this study (Ref. CEI 1057). Every effort was made to minimize animal suffering.

Thirty-three female BALB/c mice, 10 weeks old from Charles Rivers Laboratories, were randomly allocated into four experimental groups: Untreated (n = 9), Infection control (n = 6), eGFP (n = 9), and eGFP-Fh3Tq (n = 9). Groups eGFP and eGFP-Fh3Tq received a prime-boost immunization regimen (days 0 and 21) of 10 µg mRNA encoding either eGFP alone or eGFP fused to three *F. hepatica* MHCII T cell epitopes (Fh3Tq), formulated in SLN intramuscularly with a 30G needle. Control groups received equivalent volumes of Dulbecco 's-modified phosphate-buffered saline (DPBS) at the same time points. The experimental design is summarized in Fig. 1.

Sampling and challenge schedule

Peripheral blood was collected at three time points. On days 1 and 42, samples were obtained for immune response profiling by flow cytometry (using innate and adaptive flow cytometry panels, respectively). At day 42 post-vaccination, three mice per group from the Untreated, eGFP, and eGFP-Fh3Tq groups were humanely sacrificed for spleen harvest and intracellular cytokine staining (ICS) of splenocytes. Spleen suspensions were prepared by homogenizing spleens in PBS with a 21G syringe, followed by filtration through a 70 µm cell strainer, then frozen in FBS + 10% DMSO, and stored in liquid nitrogen until further analysis. The remaining 6 mice per group (except the untreated control) were orally challenged with 7 *F. hepatica* metacercariae (Ridgeway Research Ltd., St Briavels, U.K.) via oral gavage. Metacercariae viability was confirmed by stereomicroscopy observation before infection. At day 21 post-challenge, peripheral blood was collected and serum stored for ELISA anti-*F. hepatica* excretory-secretory products.

Mice were monitored daily for clinical signs and mortality throughout the post-challenge period. Deaths were recorded as they occurred for survival analysis until all mice in the infection control group died from the challenge. Surviving mice were humanely euthanized by intraperitoneal injection of sodium pentobarbital (60 mg/kg) using 30-gauge needles. All animals were subjected to necropsy. Adult flukes were recovered from the bile ducts and hepatic parenchyma and counted. Liver pathology was independently scored by two researchers blinded to group allocation. A composite liver damage score (maximum 14 points) was calculated based on changes of four macroscopic parameters: size, color, consistency, and scarring/surface lesions; each graded from 0 (non-affected) to 3 (severe, more than ¾ of the liver), with an additional point added for bile duct dilation and another for vascular damage.

Immunophenotypic studies

Whole peripheral blood (50 µL) was processed using a standardized stain-lyse-wash protocol. Briefly, individual blood and spleen samples were first washed with PBS (pH 7.4) and centrifuged at 540 × g for 5 min to remove the supernatant. All samples were pre-incubated for 30 minutes at room temperature with CD3 PE-Fire700, anti-CD45 conjugated to either PerCP or BUV496 for sample barcoding, Zombie

NIR viability dye (BioLegend, San Diego, CA, 1:2000 dilution), TruStain FcX™ PLUS, and True-Stain Monocyte Blocker. Samples were then washed with a washing solution (PBS containing 0.2% BSA, 0.1% sodium azide, and 2 mM EDTA (pH 7.4)) and centrifuged at 540 × g for 5 min. After incubation, samples were washed with washing solution and centrifuged at 540 × g for 5 min. Surface markers corresponding to the antibody panel (Supplementary Table 1) were then added together with Brilliant Stain Buffer Plus (BD Biosciences, San Jose, CA) and incubated for 30 min at RT, protected from light. Red blood cells were lysed, and leukocytes were fixed in 2 mL of 1x BD FACS Lysing Solution for 10 minutes at room temperature, then washed twice in washing solution, each wash followed by centrifugation at 540 × g for 5 min. The samples were then resuspended in 400 µL of PBS before acquisition in the flow cytometer.

Intracellular cytokine determination

Cryopreserved splenocytes were thawed rapidly in a 37°C water bath and immediately transferred to pre-warmed complete RPMI 1640 medium supplemented with 10% heat-inactivated fetal calf serum (FCS), 1% L-glutamine, and 1% penicillin/streptomycin. A total of 0.25×10^6 cells per well were plated in 96-well flat-bottom plates and rested for 24 h at 37°C, 5% CO_2 prior to *ex vivo* stimulation. Cells were stimulated with a pool of the peptides that compose Fh3Tq (PepPower™ Chemical Peptide Synthesis GenScript Biotech B.V., Rijswijk, Netherlands) at a concentration of 10 µg/mL per peptide or phorbol 12-myristate 13-acetate (PMA; 25 ng/mL; Sigma-Aldrich, P-8139) and ionomycin (900 ng/mL; Sigma-Aldrich, I-0634) as a positive control. Unstimulated wells served as negative controls. To facilitate intracellular cytokine analysis and maintain surface marker integrity, all cells were treated with Brefeldin A (10 µg/mL; Sigma-Aldrich, B7651) to inhibit Golgi-mediated protein transport, and therefore cytokine secretion, and TAPI-2 (20 µM; Sigma-Aldrich, SML0420) to block TACE/ADAM17 protease, thereby preventing activation-induced CD62L shedding. Additionally, anti-CD28 (1 µg/mL; Thermo Fisher Scientific, 16-0281-82) as a co-stimulatory signal. After a 6h incubation, cells were harvested, washed with PBS, and surface markers were stained using the same protocol described above with their corresponding panel (Supplementary Table 1). For intracellular cytokine staining, instead of performing a lysis and fixation step with BD FACS Lysing Solution, the cells were washed with washing solution and fixed with 100 µL of Fixation Solution from the Fix & Perm™ Cell Permeabilization Kit (ThermoScientific, Cat#GAS003) for 15 min at RT, washed again, and then 100 µL of Permeabilization Solution was added, along with antibodies against IFNγ, IL-4, IL-17A, and IL-22 (Supplementary Table 1). After 15 min of incubation at RT, samples were washed with washing solution and resuspended in 300 µL of PBS for acquisition. The frequency of cytokine-producing subpopulations was expressed as percentages of their respective parent populations. Where sufficient samples were available, all conditions were performed in duplicate and then averaged before statistical analysis.

Flow cytometry data acquisition and analysis

Cytometry acquisition was performed on an Aurora spectral flow cytometer (Cytek, Fremont, CA) equipped with five lasers (355 nm, 405 nm, 488 nm, 561 nm, 640 nm). Daily instrument setup and quality

control were performed using SpectroFlo QC beads (Cytek) according to the manufacturer's instructions before sample measurement. To ensure accurate spectral unmixing, single-stained reference controls for each fluorochrome in the antibody panel, along with an unstained control sample, were processed identically to the multicolor-stained samples (Supplementary Table 2). The resulting unmixing matrix was generated using SpectroFlo software (v3.3.0; Cytek). The accuracy of the unmixing was assessed by comparing its performance with single-stained references and the full-stained sample using NxN plots.

For flow cytometric data analysis, initial gating excluded dead cells based on Zombie NIR live/dead marker expression, and a parameter *vs.* time plot was employed to exclude events exhibiting unstable acquisition signal fluctuation (e.g., due to start-up/end of acquisition or clogs). Subsequently, doublets were removed by gating on forward scatter area (FSC-A) versus forward scatter height (FSC-H). Non-lysed red blood cells were excluded from the analysis using the side scatter (SSC) signal from both the blue and violet lasers. Leukocytes were defined as CD45-positive cells. Specific immune cell populations were identified based on their immunophenotypic profiles, as detailed elsewhere[18] and in Supplementary Table 3. T-cell differentiation states were stratified using a combinatorial expression pattern of CD27, CD44, and CD62L. Within this framework, the naïve compartment was identified as $CD27^{+}CD44^{-}CD62L^{+}$, while memory cells were broadly categorized as CM + EM based on CD44 acquisition. Terminally differentiated EMRA cells were distinguished by the loss of CD27 and CD62L alongside a $CD44^{-}$/lo phenotype. For identification of cytokine-producing cells, singlets and viable lymphocytes were gated, and non-T cells were excluded ($B220^{+}$, $NKp46^{+}$). Afterward, $TCR\beta^{+}$ cells were subdivided into $CD4^{+}$ (Th) and $CD8^{+}$ (Tc) populations. Within these, functional subsets were defined using Boolean gating based on intracellular cytokine expression as Th1/Tc1 ($IFN\gamma^{+}$ $IL\text{-}4^{-}$ $IL\text{-}17A^{-}$), Th2 ($IL\text{-}4^{+}$ $IFN\alpha^{-}$ $IL\text{-}17A^{-}$), Th17/Tc17 ($IL\text{-}17A^{+}$ $IFN\alpha^{-}$ $IL\text{-}4^{-}$), and Th1/Th17 ($IFN\alpha^{+}$ $IL\text{-}17A^{+}$), with IL-22 expression analyzed as an additional functional marker. Cytokine-producing B cells were identified as TCRβ- $B220^{+}$ lymphocytes $IFN\gamma^{+}$ or $IL\text{-}4^{+}$, respectively. All flow cytometric data were analyzed using Infinicyt software version 2.1.0.a (BD Biosciences, San Jose, CA, USA).

Antibody evaluation against vaccination and F. hepatica excretory/secretory antigens by ELISA

IgG antibodies in serum were quantified by indirect enzyme-linked immunosorbent assay (ELISA). Flat-bottom 96-well polystyrene plates were coated with 100 µL/well of either *F. hepatica* excretory-secretory (ES) antigen at 4 µg/mL or individual synthetic T-cell peptides at 1 µg/mL, diluted in carbonate-bicarbonate coating buffer (15 mM Na_2CO_3, 35 mM $NaHCO_3$, pH 9.6). Plates were sealed and incubated overnight (12–18 h) at 4°C. Non-specific binding sites were blocked with 2% bovine serum albumin (BSA) in PBS-T (PBS + 0.05% Tween 20, pH 7.2) at 100 µL/well for 1 h at 37°C. Plates were then washed three times with PBS-T (3 min per wash).

Serum samples were diluted 1:100 in PBS-T, added at 100 µL/well in technical duplicates, and incubated for 1 h at 37°C. After three washes, horseradish peroxidase (HRP)-conjugated anti-mouse IgG secondary antibody (A9044, Sigma-Aldrich, San Luis, MI, USA) diluted 1:2000 in PBS-T was added at 100 µL/well and incubated for 1 h at 37°C. Following three additional washes, the enzymatic reaction was developed

by adding 100 µL/well of substrate solution containing o-phenylenediamine (OPD, 0.265 mg/mL) and 0.04% (v/v) H_2O_2 in citrate-phosphate buffer (25 mM citric acid, 25 mM Na_2HPO_4, pH 5.0). Plates were incubated in the dark for 2–10 min, and the reaction was stopped with 50 µL/well of 3 N H_2SO_4. Optical density (OD) was read at 492 nm using a microplate reader. Seropositivity was defined as OD values exceeding the cutoff computed as the median plus three times the median absolute deviation (MAD) of the uninfected control group.

Statistics and data analysis

All statistical analyses were performed in R (v 4.5.2) using the packages “survival” [22], “survminer” [23], “rstatix” [24], and “ggpubr” [25]. All plots were generated with “ggplot2” [26].

Survival was estimated by the Kaplan-Meier method and compared across groups using the log-rank test; pairwise group comparisons were performed with BH-adjusted log-rank tests. For all continuous variables, the Kruskal-Wallis rank-sum test was used, followed by pairwise Wilcoxon rank-sum tests when significant. A significance threshold of 0.05 was applied throughout, and p-values from multiple comparisons were adjusted by the Benjamini-Hochberg (BH) method to control the false discovery rate[27] unless otherwise stated. For flow cytometry data, outliers were identified prior to analysis as those exceeding 2.5 times the interquartile range and excluded from downstream testing

Results

eGFP-Fh3Tq mRNA is translated in vitro and efficiently complexed in SLN-based vectors

We first verified the *in vitro* expression of the eGFP-Fh3Tq mRNA construct, in which three T cell epitopes from *F. hepatica* (T14, T15, and T16) were fused to the C-terminus of eGFP. HEK-293T cells were transfected with either eGFP or eGFP-Fh3Tq mRNA using Lipofectamine MessengerMAX at two doses (2.5 and 5 µg per well) and assessed by flow cytometry 24 h post-transfection. Both constructs achieved high transfection efficiency across doses, with 95.51% and 80.64% eGFP-positive cells at 2.5 µg/well, and 99.72% and 87.88% eGFP-positive cells at 5 µg/well for eGFP and eGFP-Fh3Tq, respectively. Although the eGFP-Fh3Tq mRNA reached high levels of transfection, the median fluorescence intensity was approximately 0.15-fold that of the eGFP control (Fig. 2.a). Western blot analysis using a C-terminal anti-His-tag antibody confirmed that the eGFP-Fh3Tq fusion protein was expressed as a single band at the expected molecular weight (~ 36 kDa) (Fig. 2.b).

To deliver the multiepitope mRNA construct *in vivo*, we formulated it into an SLN vector comprising a a Precirol® ATO 5 solid core surrounded by a layer of surfactants containing the cationic lipid DOTAP, protamine as a nucleic acid condensing agent, and HA as an outer polysaccharide shell. Bare SLN showed a particle size of 143.3 ± 2.19 nm, a PDI of 0.26 ± 0.01, and a surface charge of + 60.13 ± 1.54 mV. Upon the addition of the mRNA complexed with protamine and HA, the resulting vectors showed a moderate increase in size and a reduction in surface charge. The vector carrying the mRNA-eGFP control

construct had a mean diameter of 195.7 ± 1.0 nm (PDI = 0.26 ± 0.00, ζ-potential = + 32.62 ± 3.84 mV), while the vector carrying the mRNA-eGFP-Fh3Tq vaccine construct measured 185.7 ± 1.1 nm (PDI = 0.24 ± 0.01, ζ-potential = + 19.9 ± 0.78 mV) (Table 1).

The vectors' ability to condense and protect the mRNA cargo was assessed by agarose gel electrophoresis. Both vectors fully retained the mRNA in the loading wells, with no detectable band migration, confirming complete complexation of the nucleic acid (Fig. 2.c, lanes 5–6). Upon SDS treatment to disrupt electrostatic interactions, only partial mRNA release was observed (Fig. 2.c, lanes 7–8), as evidenced by the persistence of material in the wells and faint migrating bands. Importantly, the released mRNA migrated at the expected molecular weight, indicating that the transcript's integrity was preserved during the formulation process. RiboGreen assay confirmed that both mRNAs were strongly condensed within the vectors, with exposure percentages of 3.03 ± 0.67 and 2.34 ± 2.31 for the mRNA-eGFP vector and the mRNA-eGFP-Fh3Tq SLN vector, respectively.

Table 1
Physicochemical characterization of SLN formulations.

Formulation	**Weight ratio (w:w:w:w)**	**Size (d.nm)**	**PDI**	**Z-Potential (mV)**
SLN core	—	143.3 ± 2.19	0.26 ± 0.01	+ 60.13 ± 1.54
HA:P:eGFP mRNA:SLN	0.5:0.5:1:5	195.7 ± 1.0	0.26 ± 0.00	+ 32.62 ± 3.84
HA:P:eGFP-Fh3Tq mRNA:SLN	0.5:0.5:1:5	185.7 ± 1.1	0.24 ± 0.01	+ 19.9 ± 0.78

SLN-delivered eGFP-peptide mRNA vaccination modulates innate and adaptive immune cell populations

We then vaccinated BALB/c mice in a prime-boost regimen, separated by 21 days, with either the eGFP mRNA-SLN or the eGFP-Fh3Tq mRNA-SLN. To assess the immunological impact of vaccination, peripheral blood was analyzed by flow cytometry at two time points: day 1 and day 42 post-prime (Fig. 1). Since the untreated and infected control groups were not yet differentiated prior to challenge, only the untreated group was used as the naïve control.

Analysis of innate immune populations on day 1 showed release of inflammatory populations into peripheral blood (Fig. 3). The proportions of mature neutrophils were significantly elevated in both vaccinated groups compared to untreated controls (eGFP: 23.7 ± 4.5%, eGFP-Fh3Tq: 26.5 ± 4.5% *vs.* untreated control: 14.1 ± 2.7%; p = 0.013 for both pairwise comparisons), with no significant difference between vaccinated groups. Basophils were significantly increased in the eGFP-Fh3Tq group compared to untreated controls (1.18 ± 0.08% *vs.* 0.66 ± 0.19%; p = 0.023), with the eGFP receiving group showing an intermediate, non-significant elevation. A similar trend was observed for non-classical monocytes, which were significantly higher in the eGFP-Fh3Tq group than in the untreated control (0.87 ± 0.30% *vs.*

0.36 ± 0.26%; p = 0.026). Eosinophil frequencies tended to be higher in both vaccinated groups, although this difference did not reach statistical significance (Kruskal-Wallis p = 0.13). Taken together, these early innate responses appeared to be driven primarily by the SLN-mRNA vector itself, as both vaccinated groups showed similar patterns of activation regardless of the encoded antigen.

At day 42 post-vaccination, the profile of the adaptive immune populations diverged between eGFP and eGFP-Fh3Tq vaccinated mice (Fig. 4). Total B cells and mature B2 cells populations were significantly expanded in the eGFP group relative to the untreated control (p = 0.023 and p = 0.039, respectively) and the eGFP-Fh3Tq group (p = 0.015 and p = 0.006, respectively). Of note, B-cell frequencies in the eGFP-Fh3Tq group remained comparable to those of naïve animals, with no evidence of expansion. Consistent with this observation, indirect ELISA detected no IgG response against the synthetic peptides comprising Fh3Tq in any experimental group at day 42 (Supplementary Fig. 1). Conversely, the T-cell compartment displayed the opposite pattern. Total $CD4^+$ T helper cell frequencies tended to increase in eGFP-Fh3Tq-vaccinated animals, though this difference did not reach statistical significance (Kruskal-Wallis p = 0.075). However, terminally differentiated effector memory (EMRA) $CD4^+$ T cells were significantly higher in the eGFP-Fh3Tq group (20.1 ± 0.6%) relative to both the eGFP group (11.4 ± 1.7%; p = 0.013) and untreated controls (13.9 ± 4.0%; p = 0.045). Similarly, total $CD8^+$ T-cell frequencies were significantly higher in eGFP-Fh3Tq-vaccinated mice than in the eGFP group (10.8 ± 1.5% *vs.* 7.8 ± 1.7%; p = 0.046), and the $CD8^+$ EMRA subset showed the most pronounced difference, being significantly higher in the eGFP-Fh3Tq group than in both the eGFP and untreated control groups (p = 0.013 for both comparisons).

Vaccination induces a Th1 and Th17 skewed cytokine profile

To characterize the antigen-specific T cell response induced by eGFP-Fh3Tq vaccination, splenocytes from immunized and control mice were restimulated with the vaccine peptides (T14 + T15+T16) and cytokine production was assessed at the single-cell level by intracellular cytokine staining. $CD4^+$ T cell responses were evaluated by quantifying four functionally defined, mutually exclusive populations: Th1 ($IFN\gamma^+$/IL-4^-IL-$17A^-$), Th2 (IL-4^+/$IFN\gamma^-$/IL-$17A^-$), Th17 (IL-$17A^+$/$IFN\gamma^-$/IL-4^-), and Th22 (IL-22^+/$IFN\gamma^-$/IL-4^-). $CD8^+$ T cell responses were evaluated by quantifying Tc1 ($IFN\gamma^+$/IL-$17A^-$) and Tc17 (IL-$17A^+$/IFNγ-) populations, and $IFN\gamma^+$ and IL-4^+ B cells were also evaluated (Fig. 5). Polyclonal stimulation with PMA+ionomycin revealed a broadly expanded cytokine-competent T cell pool in all groups, consistent with its TCR-independent mechanism of activation. Given the limited sample size (n = 3 per group), these results are presented as exploratory; Kruskal-Wallis p-values are provided for reference, but statistical power is insufficient for robust pairwise comparisons.

Upon peptide stimulation, $CD4^+$ T cells from eGFP-Fh3Tq-vaccinated mice showed a tendency toward a Th1 and Th17 profile (Fig. 5.a). Th1 $CD4^+$ cells (0.39 ± 0.08%) reached approximately twice the frequency observed in naïve and eGFP-vaccinated mice (Untreated, 0.18 ± 0.13%; eGFP, 0.15 ± 0.06%; Kruskal-Wallis p = 0.118). Th17 $CD4^+$ cells followed a similar pattern, with the Fh3Tq group reaching a threefold

increase over controls (Untreated, 0.07 ± 0.05%; eGFP, 0.07 ± 0.02%; eGFP-Fh3Tq, 0.20 ± 0.07%; Kruskal-Wallis p = 0.113). Of note, Th2 and Th1/17 cells ($IFN\gamma^+$/$IL\text{-}17A^+$) were detected across all groups at very low frequencies, and no vaccine-specific expansion was observed in either population. Similarly, no vaccine-specific differences were detected in the Th22 compartment. Interestingly, mice vaccinated with eGFP-Fh3Tq also showed a trend toward higher levels of polyclonal stimulation across Th1, Th2, and Th17 populations.

The most notable antigen-specific response was observed in the $CD8^+$ compartment (Fig. 5b). $CD8^+$ Tc1 cells in the eGFP-Fh3Tq group reached 0.90 ± 0.84%, a sixfold increase over control mice (Untreated, 0.15 ± 0.07%) and three times higher than the eGFP group (eGFP, 0.26 ± 0.04%; Kruskal-Wallis p = 0.113). However, individual animals showed varied responses, with one mouse responding poorly, as reflected in the standard deviation. Similarly, Tc17 $CD8^+$ cells showed a modest increase in the eGFP-Fh3Tq group (0.18 ± 0.11% *vs.* 0.07 ± 0.08% in unstimulated samples; Kruskal-Wallis p = 0.329), with one mouse showing only a slight response. When cytokine-producing cells were aggregated within each lymphocyte compartment, the $CD8^+$ compartment showed the most pronounced vaccine effect upon peptide stimulation (Kruskal-Wallis p = 0.039), driven by higher total cytokine production in the eGFP-Fh3Tq group (1.08 ± 0.75%) relative to untreated (0.22 ± 0.08%) and eGFP controls (0.34 ± 0.05%), although pairwise comparisons did not reach significance after correction (p.adj = 0.121). Antigen-specific Th1, Th17, Tc1 and Tc17 cells in eGFP-Fh3Tq-vaccinated mice were distributed across both the central/effector memory (CM + EM) and terminally differentiated effector memory (EMRA) compartments, with CM + EM cells accounting for approximately half of the antigen-specific response in each subset (Th1, 49.7 ± 23.1%; Th17, 52.0 ± 17.6%; Tc1, 66.3 ± 20.6%; Tc17, 57.9 ± 21.2% of total antigen-specific $CD4^+$ and $CD8^+$ T cells, respectively).

Among B cells (Fig. 5.c), the data suggest that mice vaccinated with eGFP-Fh3Tq have higher baseline production of IL-4 under all conditions, even without stimulation. Additionally, eGFP-Fh3Tq B cells exhibited a slight increase in IFNγ production when stimulated with either PMA/ionomycin or the peptide pool compared to control groups. Overall, the intracellular cytokine data support a Th1 and Th17 profile in the lymphocytes of eGFP-Fh3Tq-vaccinated mice, indicating a T cell-mediated mechanism independent of humoral responses.

eGFP-Fh3Tq mRNA vaccination improves survival and reduces hepatic pathology following Fasciola hepatica challenge

To evaluate the protective capacity of the mRNA construct, immunized mice were orally challenged with 7 *F. hepatica* metacercariae 42 days after the first vaccine dose and monitored during the infection. All mice in the unvaccinated group died of infection by day 31 post-infection (DPI), as did 5 of 6 mice in the eGFP group (pairwise log-rank test, eGFP *vs.* Infection, p = 0.834). In contrast, mice vaccinated with eGFP-Fh3Tq mRNA showed improved survival, with 4 out of 6 animals (67%) surviving to the experiment endpoint. Kaplan-Meier survival analysis revealed significant differences among groups (log-rank test, χ^2=15.2, df = 3, p = 0.002) (Fig. 6.a). This difference was statistically significant compared with the

infection control (pairwise log-rank test, eGFP-Fh3Tq *vs.* Infection, p = 0.037) and approached significance relative to the eGFP group (eGFP-Fh3Tq *vs.* eGFP, p = 0.096). Regarding the observed-to-expected event ratios, the eGFP-Fh3Tq group experienced only 2 deaths, compared with 3.75 expected, whereas both the infection control (6 observed *vs.* 2.59 expected) and eGFP (5 observed *vs.* 2.38 expected) groups exceeded their expected mortality. These differences suggest that the protective effect is attributable specifically to the Fh3Tq peptides, rather than to eGFP or the SLN vector alone. All infected mice developed anti-*Fasciola* antibodies during infection, and anti-FhES IgG levels did not differ significantly across the three challenged groups (Kruskal-Wallis, p = 0.143). Mean OD in the eGFP-Fh3Tq group trended lower than in infection controls (0.42 vs 0.54; pairwise Wilcoxon, p = 0.27) (Fig. 6b).

Worm recovery at necropsy was reduced in the eGFP-Fh3Tq group relative to infection controls (Table 2). Mean worm burden per animal was 0.7 ± 0.3 in the eGFP-Fh3Tq group, meaning a 71.4% reduction compared to the infection control (2.3 ± 1.1), while the eGFP group showed only a marginal decrease (2.0 ± 1.1; 14.3% reduction). However, the overall Kruskal-Wallis test was not significant (p = 0.112), and no pairwise comparisons were significant after Benjamini-Hochberg correction, reflecting the high inter-individual variability and the low recovery rate across all infected groups.

In line with the previous result, the sum of hepatic lesion score differed significantly between these groups (Kruskal-Wallis, p = 0.015), with mean scores of 11.3 ± 2.3 points for infection controls, 9.7 ± 2.1 for eGFP, and 6.3 ± 2.7 for eGFP-Fh3Tq, corresponding to reductions of 14.7% and 44.1% relative to infection controls. Pairwise Wilcoxon rank-sum tests (BH-adjusted) showed that both the infection control and eGFP groups differed significantly from uninfected mice (p.adj = 0.028 for both), whereas the eGFP-Fh3Tq group did not reach significance against uninfected controls (p.adj = 0.057), suggesting that livers (Supplementary Fig. 2) from peptide-vaccinated mice were closer to the uninfected condition than to infected controls.

Table 2
Recovered flukes and assessment of macroscopic hepatic lesions in mice immunised with mRNA candidates and challenged with *F. hepatica* metacercariae.

Treatment	**Worm burden**			**Hepatic damage**		
	Flukes recovered in individual mice	**Worm recovery (Mean ± SEM)**	**Reduction (%)**	**Hepatic lesion in individual mice**	**Lesion score (Mean ± SEM)**	**Reduction (%)**
Untreated	—	—	—	—	—	—
Infection	0, 2, 6, 0, 5, 1	2.3 ± 1.1	—	14, 13, 13, 0, 14, 14	11.3 ± 2.3	—
eGFP	0, 0, 0, 3, 2, 7	2.0 ± 1.1	14.3	12, 0, 9, 14, 9, 14	9.7 ± 2.1	14.7
eGFP-Fh3Tq	0, 2, 1, 0, 1, 0	0.7 ± 0.3	71.4	0, 11, 12, 14, 1, 0	6.3 ± 2.7	44.1

Discussion

This study provides the first evidence that an mRNA vaccine encoding *F. hepatica* T-cell epitopes confers protection against infection in mice. Vaccination with Fh3Tq fused to eGFP and delivered via mRNA improved survival following challenge infection. The majority of peptide-vaccinated mice survived to the experimental endpoint, whereas all infection controls and nearly all eGFP-only controls died. This protection was associated with a trend toward reduced worm burden and lower hepatic damage scores in the vaccinated group. The observed survival advantage was attributable specifically to the Fh3Tq peptides, as eGFP mRNA alone provided no detectable benefit. Notably, these same epitopes (T14, T15, and T16), when administered as synthetic peptides in the ADAD vaccination system with the immunomodulator AA0029, produced a comparable increase in survival and a similar reduction in hepatic lesion scores [28]. The consistency of these results using two distinct delivery platforms supports the conclusion that these epitopes possess protective potential. The carrier-based strategy is conceptually analogous to earlier work by Muro et al. (2007), who fused T cell epitopes from the *F. hepatica* fatty acid-binding protein Fh15 to GST to enhance immunogenicity in a recombinant protein context [9]. This principle is extended to the mRNA platform, where the carrier protein allows expression of the multipeptide constructs. A logical next step would be to replace eGFP, which lacks parasitological relevance, with a parasite-derived scaffold protein such as GST or a truncated FABP, thereby generating a bifunctional construct that serves as both a carrier and an additional antigen source.

The tested SLN-based vectors efficiently complexed the mRNA and elicited an innate immune response following vaccination, characterized by the mobilization of mature neutrophils, basophils, and non-classical monocytes into peripheral blood. This early inflammatory signature was primarily driven by the vector itself or the presence of unmodified mRNA, rather than by the encoded antigen. This observation aligns with the known immunostimulatory activity of cationic DOTAP-containing nanoparticles, which activate dendritic cells and promote type 1 immune responses [29], as well as hyaluronic acid, which facilitates CD44-mediated uptake by macrophages and dendritic cells [30,31], and the engagement of pattern recognition receptors by unmodified mRNA [32]. A similar innate activation pattern was observed with a full-length Fh15 FABP mRNA formulated in SM-102 lipid nanoparticles [18], which showed higher percentages of proinflammatory populations. Notably, despite a lesser degree of innate activation, mRNA-SLN induced an adaptive response. This finding suggests that a strong early innate response may not be necessary for subsequent T-cell priming, positioning the SLN as an alternative for mRNA delivery with reduced reactogenicity. Furthermore, in contrast to conventional ionizable LNPs used in COVID-19 vaccines and most mRNA vaccines, which require microfluidic mixing, the SLN system is based on a solid lipid core (Precirol ATO 5), with DOTAP and protamine as condensing agents, and hyaluronic acid as a functional corona, assembled through electrostatic interactions. This formulation approach may offer advantages in terms of manufacturing simplicity and cost, considerations that are particularly relevant for vaccines targeting neglected tropical diseases.

Beyond innate activation, eGFP-Fh3Tq-vaccinated mice exhibited a clear shift toward T-cell effector differentiation, with increases in both total $CD4^+$ helper and $CD8^+$ T-cell frequencies, particularly within their respective terminally differentiated effector memory (EMRA) subsets. Of note, despite the bulk T cell population expansion correspond to terminally differentiated effector memory cells, when antigen-specific T cell data were pooled across replicates to circumvent the limited number of events per individual sample, peptide-responsive Th1, Th17, Tc1 and Tc17 cells were found to comprise both EMRA and central/effector memory populations in approximately equal proportions, suggesting that eGFP-Fh3Tq vaccination drives the simultaneous generation of terminally differentiated effectors and memory populations poised for long-term protective surveillance. However, given the exploratory nature of this pooled analysis, these findings should be interpreted with caution.

Although no direct relationship between $CD4^+$ or $CD8^+$ cells and protection against *F. hepatica* infection has been described, it is known that the parasite and its products actively deplete peripheral $CD4^+$ and $CD8^+$ T-cell populations and downregulate CD4 surface expression on human T cells [33]. Presence of effector memory cells is related to the resistance in several other parasites, such as *Leishmania* or *Trypanosoma cruzi* [34,35]. This shift was not observed in the group that received mRNA encoding eGFP alone, which, in contrast, showed increases in total B cells and mature B2 cells. The group eGFP-Fh3Tq construct did not show this difference, and even though we cannot disregard a specific peptide effect on this response-switch, it might simply be attributable to the lower level of expression of the construct, as we observed *in vitro*. Higher expression may be required to elicit a humoral response, whereas lower levels may suffice for T-cell priming. Additionally, this pattern could reflect the intrinsic immunogenicity of eGFP as a foreign protein, which, in the absence of T-cell polarizing peptides, follows the default pathway of T-dependent humoral response. The incorporation of Fh3Tq peptides appears to skew $CD4^+$ T-cell differentiation toward Th1 and Th17 effector differentiation rather than Tfh polarization, which could reduce Tfh-mediated help to B cells and thereby limit B-cell expansion, consistent with the mutual exclusivity of Th1 and Tfh fates and the role of Tfh cells in germinal-center B-cell help[36,37]. This interpretation is consistent with the absence of detectable antigen-specific antibodies in eGFP-Fh3Tq-vaccinated mice, and supports the conclusion that protection in this model is mediated by cellular rather than humoral immunity.

In line with this, the cytokine profile induced by eGFP-Fh3Tq vaccination was dominated by IFNγ and IL-17 responses, with no detectable Th2 component. Upon peptide restimulation of splenocytes, $CD4^+$ T cells from vaccinated mice showed consistent increases in IFNγ and IL-17A production relative to both control groups, and a pronounced IFNγ response was also observed in $CD8^+$ T cells. This Th1 and Th17-skewed profile aligns with the type of immunity considered protective against *Fasciola* infection. *F. hepatica* actively suppresses Th1 and Th17 responses as part of its survival strategy, and vaccines that maintain or restore these pathways have been associated with improved outcomes [38,39]. At the transcriptomic level, Rojas-Caraballo et al. (2017) previously reported upregulation of IL-12 signaling, iNOS, and reactive oxygen species pathways in splenocytes from mice vaccinated with these same peptides in the ADAD system. The present antigen-specific cytokine production data provide protein-level

confirmation of this Th1 bias and extend these findings by identifying a Th17 component and a $CD8^+$ Tc1 response, either not captured in the earlier transcriptomic analysis or induced by the different delivery platform. However, it should be noted that the intracellular cytokine analysis was performed on a small number of animals per group, which limits statistical power; accordingly, these data should be regarded as exploratory and hypothesis-generating rather than confirmatory.

The mechanistic basis for Th1-mediated protection likely involves the activation of classically activated (M1) macrophages which is driven by IFNγ, the principal signal for macrophage polarization toward the M1 phenotype [40], which produces nitric oxide and reactive oxygen species that kill newly excysted juveniles [41]. In the bovine host, macrophage-mediated killing of NEJ has been shown to be directly proportional to nitric oxide production [42], and this mechanism underlies the natural resistance of Indonesian Thin-Tail sheep to *F. gigantica* [43]. Our vaccine generates IFNγ from both $CD4^+$ Th1 and $CD8^+$ Tc1 cells, which would converge on this effector pathway. The Th17 component may further contribute to protection by increasing neutrophil recruitment to sites of parasite migration[44]. The induction of cytotoxic $CD8^+$ T cells by peptides originally selected as MHC class II binders is notable and suggests that the encoded antigen enters the classical MHC class I processing pathway directly in transfected cells or is presented by dendritic cells through uptake of cellular debris [12,45]. This contrasts with protein-based vaccination against *F. hepatica*, where the adaptive response is dominated by $CD4^+$ T helper cells with minimal $CD8^+$ engagement [46]. The endogenous expression achieved by mRNA vaccination might enable the generation of $CD8^+$ cytotoxic responses against an extracellular parasite, inducing Th1 and Th17 responses via a mechanism not typically addressed by *Fasciola* evasion repertoire that focuses on $CD4^+$ inhibition [47]. The use of unmodified nucleotides in the mRNA, rather than N1-methylpseudouridine, may further contribute to this $CD8^+$ bias. Recent comparative studies have shown that unmodified mRNA favors IFNα and IL-7 induction along with stronger $CD8^+$ IFNγ responses [32]. Among B cells, eGFP-Fh3Tq-vaccinated mice showed a consistent elevation in IFNγ-producing B cells upon peptide stimulation. This phenotype is characteristic of Th1-polarized immune environments [48] and may serve as an indirect marker of the overall type 1 response generated by vaccination.

No anti-peptide IgG antibodies were detected in any group, which is consistent with the Fh3Tq construct encoding exclusively small MHC class II-restricted T-cell epitopes that do not necessarily induce a B-cell response. The absence of a humoral response contrasts with the Fh15 FABP mRNA-LNP vaccine [18] and Sm-TSP-2 mRNA vaccine [14], which encode full-length proteins and elicit both cellular and antibody responses, where protection correlated with IgG levels. Further studies discuss whether signal peptides are needed to develop proper humoral responses in some mRNA vaccines[49]. The absence of IgG-mediated protection is worth placing in the context of fasciolosis vaccine development, although resistance to infection in natural hosts has been associated with an IgG2 production and robust type 1 cytokine profile [50]. It is unclear whether the protection depends on IgG2 or serves as a marker of the Th1 response [51]. The correlation between antibody titers and actual protection against *F. hepatica* has been inconsistent across trials. Several vaccination studies in ruminants have failed to find significant

correlations between antigen-specific IgG levels and reductions in worm burden, and, paradoxically, formulations using Th2-biased adjuvants such as alum have occasionally outperformed Th1-oriented adjuvants in eliciting protection despite generating lower IgG2 responses [52]. Our data contribute to this picture by demonstrating that protection can be achieved in the complete absence of detectable anti-parasite antibodies, at least in the murine model.

In summary, this study provides the first evidence that an mRNA vaccine encoding defined T-cell epitopes of *F. hepatica* can confer protection against experimental infections. The eGFP fusion strategy, initially developed to address poor expression of small peptide constructs in mRNA format [11], demonstrated functional efficacy in a vaccination context. The resulting Th1- and Th17-skewed immune profile, along with the induction of $CD8^+$ cytotoxic responses, aligns with the immunological requirements for protection against this parasite and indicates that endogenous antigen expression via mRNA delivery may be particularly suitable for vaccines targeting tissue-dwelling helminths, where cellular immunity is central. Future research should prioritize validation in natural infection hosts such as cattle or sheep, dose optimization, and replacement of eGFP with a parasite-derived carrier protein to generate bifunctional constructs. The modularity of the mRNA platform also allows for the straightforward incorporation of additional T-cell epitopes from other *F. hepatica* antigens, which may further enhance protective efficacy. Collectively, these findings establish a foundation for developing mRNA-based vaccines against fasciolosis and, more broadly, helminth infections in which T-cell-mediated immunity is the primary correlate of protection.

Data Availability

The processed datasets generated and analyzed during the current study, along with the code used for this purpose, are available in the Zenodo repository at https://doi.org/10.5281/zenodo.19613320. Raw flow cytometry files (.fcs) are available from the corresponding authors upon reasonable request.

Declarations

Competing Interests

JP is an employee of Cytognos/Water Biosciences (formerly BD Biosciences), Salamanca, and declares no non-financial competing interests. MG-B is cofounder and has a significant equity stake in Circurna, Inc, which is commercializing RNA-based vaccines and therapies, and declares no non-financial competing interests. All other authors declare no financial or non-financial competing interests

Author Contributions Statement

JS-M, TS, and MG-B designed, produced, and characterized the mRNA constructs. MAS and AdPR designed and developed the solid lipid nanoparticle delivery platform, formulated and characterized the

loaded SLNs, and participated in study planning. JS-M, JL-A, RM-R, BV, and AM planned and performed the in vivo immunization, challenge, and parasitological experiments. CT and JP designed and performed the flow cytometry experiments, including intracellular cytokine staining, and carried out the associated data analysis. JS-M, JL-A, and CT performed the statistical analysis and drafted the manuscript. RM-R, MG-B, and AM acquired funding. BV and AM jointly supervised the study as senior authors. All authors reviewed and approved the final version of the manuscript.

Author Contribution

JS-M, TS, and MG-B designed, produced, and characterized the mRNA constructs. MAS and AdPR designed and developed the solid lipid nanoparticle delivery platform, formulated and characterized the loaded SLNs, and participated in study planning. JS-M, JL-A, RM-R, BV, and AM planned and performed the in vivo immunization, challenge, and parasitological experiments. CT and JP designed and performed the flow cytometry experiments, including intracellular cytokine staining, and carried out the associated data analysis. JS-M, JL-A, and CT performed the statistical analysis and drafted the manuscript. RM-R, MG-B, and AM acquired funding. BV and AM jointly supervised the study as senior authors. All authors reviewed and approved the final version of the manuscript.

Acknowledgement

We thank Lidia Silo and Silvia Martín (Cytometry Service, NUCLEUS, University of Salamanca) for their technical assistance with flow cytometry acquisition and instrument setup, and Alicia Rodríguez-Gascón, Paula Fernández-Muro, and Madalen Arribas-Galarreta (University of the Basque Country, UPV/EHU) for their support in the preparation and characterization of the solid lipid nanoparticles.Financial support from PID2022-136462NB-I00 funded by “Ministerio de Ciencia e Innovación” and cofinanced by “European Union”. TS and MG-B Acknowledge funding from the University of Virginia. JS-M acknowledges the predoctoral fellowship program of Junta de Castilla y León, co-funded by “Fondo Social Europeo” (Orden EDU875/2021). CT was supported by an Andrés Laguna fellowship (Junta de Castilla y León, co-financed by the Fondo Social Europeo Plus, FSE+; ORDEN EDU/300/2025) and a Miguel Servet grant from the Instituto de Salud Carlos III (ISCIII) (CP25/00087), co-funded by the European Social Fund Plus (ESF+). MAS and AdP-R acknowledge the funding from the Department of Education of the Basque Government (IT1587-22,GIC21/34). The funders played no role in study design, data collection, analysis and interpretation of data, or the writing of this manuscript.

Data Availability

The processed datasets generated and analyzed during the current study, along with the code used for this purpose, are available in the Zenodo repository at https://doi.org/10.5281/zenodo.19613320. Raw flow cytometry files (.fcs) are available from the corresponding authors upon reasonable request.

References

1. Mas-Coma, S., Bargues, M. D. & Valero, M. A. Human fascioliasis infection sources, their diversity, incidence factors, analytical methods and prevention measures. *Parasitology* 145, 1665–1699 (2018).
2. World Health Organization. *Fasciola: Background Document for the WHO Guidelines for Drinking-Water Quality and the WHO Guidelines on Sanitation and Health*. https://iris.who.int/handle/10665/380677 (2025) doi:10.2471/b09245.
3. Mehmood, K. *et al.* A review on epidemiology, global prevalence and economical losses of fasciolosis in ruminants. *Microb Pathog* 109, 253–262 (2017).
4. Kelley, J. M. *et al.* Current Threat of Triclabendazole Resistance in *Fasciola hepatica*. *Trends Parasitol* 32, 458–469 (2016).
5. Fairweather, I., Brennan, G. P., Hanna, R. E. B., Robinson, M. W. & Skuce, P. J. Drug resistance in liver flukes. *International Journal for Parasitology: Drugs and Drug Resistance* 12, 39–59 (2020).
6. Ryan, S., Shiels, J., Taggart, C. C., Dalton, J. P. & Weldon, S. *Fasciola hepatica*-Derived Molecules as Regulators of the Host Immune Response. *Front Immunol* 11, 2182 (2020).
7. Rufino-Moya, P. J. *et al.* Advancement in Diagnosis, Treatment, and Vaccines against *Fasciola hepatica*: A Comprehensive Review. *Pathogens* 13, 669 (2024).
8. Malonis, R. J., Lai, J. R. & Vergnolle, O. Peptide-based vaccines: Current progress and future challenges. *Chem Rev* 120, 3210–3229 (2020).
9. Muro, A. *et al.* Identification of *Fasciola hepatica* recombinant 15-kDa fatty acid-binding protein T-cell epitopes that protect against experimental fascioliasis in rabbits and mice. *J Parasitol* 93, 817–823 (2007).
10. Rojas-Caraballo, J. *et al. In vitro* and *In vivo* Studies for Assessing the Immune Response and Protection-Inducing Ability Conferred by *Fasciola hepatica*-Derived Synthetic Peptides Containing B- and T-Cell Epitopes. *PLoS ONE* 9, e105323 (2014).
11. Sánchez-Montejo, J. *et al.* Design and Expression of *Fasciola hepatica* Multiepitope Constructs Using mRNA Vaccine Technology. *Int J Mol Sci* 26, 1190 (2025).
12. Cruz, F. M., Chan, A. & Rock, K. L. Pathways of MHC I cross-presentation of exogenous antigens. *Seminars in Immunology* 66, 101729 (2023).
13. Qin, S. *et al.* mRNA-based therapeutics: powerful and versatile tools to combat diseases. *Sig Transduct Target Ther* 7, 166 (2022).
14. de Oliveira, A. S. *et al.* mRNA vaccines encoding variant forms of Sm-TSP-2 confer protective immunity against Schistosoma mansoni. *npj Vaccines* 10, (2025).
15. de Oliveira, A. S. *et al.* Altering the intracellular trafficking of Necator americanus GST-1 antigen yields novel hookworm mRNA vaccine candidates. *PLoS Negl Trop Dis* 19, e0012809 (2025).
16. Zhang, Y. *et al.* A novel mRNA vaccine, TGGT1_278620 mRNA-LNP, prolongs the survival time in BALB/c mice with acute toxoplasmosis. *Microbiol Spectr* 12, e0286623 (2024).

17. Kunkeaw, N. *et al.* A Pvs25 mRNA vaccine induces complete and durable transmission-blocking immunity to Plasmodium vivax. *NPJ Vaccines* 8, 187 (2023).
18. Sánchez-Montejo, J. *et al.* Harnessing mRNA technology against *Fasciola hepatica*: Immunological insights from a fatty acid binding protein vaccine. *Front Immunol* 16, 1693674 (2025).
19. Baiersdörfer, M. *et al.* A Facile Method for the Removal of dsRNA Contaminant from *In vitro*-Transcribed mRNA. *Mol Ther Nucleic Acids* 15, 26–35 (2019).
20. Rodríguez-Castejón, J. *et al.* α-Galactosidase A Augmentation by Non-Viral Gene Therapy: Evaluation in Fabry Disease Mice. *Pharmaceutics* 13, 771 (2021).
21. Jones, L. J., Yue, S. T., Cheung, C.-Y. & Singer, V. L. RNA Quantitation by Fluorescence-Based Solution Assay: RiboGreen Reagent Characterization. *Analytical Biochemistry* 265, 368–374 (1998).
22. Therneau, T. M. *A Package for Survival Analysis in R*. (2024).
23. Kassambara, A., Kosinski, M. & Biecek, P. *Survminer: Drawing Survival Curves Using Ggplot2*. (2021). doi:10.32614/cran.package.survminer.
24. Kassambara, A. *Rstatix: Pipe-Friendly Framework for Basic Statistical Tests*. (2023). doi:10.32614/cran.package.rstatix.
25. Kassambara, A. *Ggpubr: Ggplot2 Based Publication Ready Plots*. (2023). doi:10.32614/cran.package.ggpubr.
26. Wickham, H. *Ggplot2: Elegant Graphics for Data Analysis*. (Springer-Verlag New York, New York, 2016).
27. Benjamini, Y. & Hochberg, Y. Controlling the false discovery rate: a practical and powerful approach to multiple testing. *Journal of the Royal Statistical Society: Series B (Methodological)* 57, 289–300 (1995).
28. Rojas-Caraballo, J. *et al.* Transcriptome profiling of gene expression during immunisation trial against *Fasciola hepatica*: identification of genes and pathways involved in conferring immunoprotection in a murine model. *BMC Infect Dis* 17, 94 (2017).
29. Vasievich, E. A., Ramishetti, S., Zhang, Y. & Huang, L. Trp2 Peptide Vaccine Adjuvanted with (*R*)-DOTAP Inhibits Tumor Growth in an Advanced Melanoma Model. *Mol. Pharmaceutics* 9, 261–268 (2012).
30. Almalik, A. *et al.* Hyaluronic acid (HA) presentation as a tool to modulate and control the receptor-mediated uptake of HA-coated nanoparticles. *Biomaterials* 34, 5369–5380 (2013).
31. Gennari, A., Pelliccia, M., Donno, R., Kimber, I. & Tirelli, N. Mannosylation Allows for Synergic (CD44/C-Type Lectin) Uptake of Hyaluronic Acid Nanoparticles in Dendritic Cells, but Only upon Correct Ligand Presentation. *Adv Healthcare Materials* 5, 966–976 (2016).
32. Soler, S., Maser, K., Zillinger, T. & Bartok, E. To modify or not to modify—That is still the question for some mRNA applications. *Molecular Therapy Nucleic Acids* 36, 102655 (2025).
33. Prowse, R. K., Chaplin, P., Robinson, H. C. & Spithill, T. W. *Fasciola hepatica* cathepsin L suppresses sheep lymphocyte proliferation *in vitro* and modulates surface CD4 expression on human and ovine

T cells. *Parasite Immunol* 24, 57–66 (2002).

34. Zaph, C., Uzonna, J., Beverley, S. M. & Scott, P. Central memory T cells mediate long-term immunity to Leishmania major in the absence of persistent parasites. *Nat Med* 10, 1104–1110 (2004).
35. Bustamante, J. M., Bixby, L. M. & Tarleton, R. L. Drug-induced cure drives conversion to a stable and protective CD8 + T central memory response in chronic Chagas disease. *Nat Med* 14, 542–550 (2008).
36. Chang, Y. *et al.* TGF-β specifies TFH versus TH17 cell fates in murine CD4 + T cells through c-Maf. *Science Immunology* 9, eadd4818 (2024).
37. Sheikh, A. A. & Groom, J. R. Transcription tipping points for T follicular helper cell and T-helper 1 cell fate commitment. *Cell Mol Immunol* 18, 528–538 (2021).
38. Corral-Ruiz, G. M. & Sánchez-Torres, L. E. *Fasciola hepatica*-derived molecules as potential immunomodulators. *Acta Tropica* 210, 105548 (2020).
39. Ramos-Nieves, R. *et al.* A Modified Variant of *Fasciola hepatica* FhSAP-2 (mFhSAP-2) as a Recombinant Vaccine Candidate Induces High-Avidity IgG2c Antibodies and Enhances T Cell Activation in C57BL/6 Mice. *Vaccines* 13, 545 (2025).
40. Yunna, C., Mengru, H., Lei, W. & Weidong, C. Macrophage M1/M2 polarization. *European Journal of Pharmacology* 877, 173090 (2020).
41. Calvani, N. E. D. *et al.* Two Distinct Superoxidase Dismutases (SOD) Secreted by the Helminth Parasite *Fasciola hepatica* Play Roles in Defence against Metabolic and Host Immune Cell-Derived Reactive Oxygen Species (ROS) during Growth and Development. *Antioxidants* 11, 1968 (2022).
42. Sulaiman, A. A. *et al.* A Trematode Parasite Derived Growth Factor Binds and Exerts Influences on Host Immune Functions via Host Cytokine Receptor Complexes. *PLoS Pathog* 12, e1005991 (2016).
43. Piedrafita, D. *et al.* Peritoneal Lavage Cells of Indonesian Thin-Tail Sheep Mediate Antibody-Dependent Superoxide Radical Cytotoxicity *In vitro* against Newly Excysted Juvenile *Fasciola gigantica* but Not Juvenile *Fasciola hepatica*. *Infect Immun* 75, 1954–1963 (2007).
44. Mazzoni, A., Maggi, L., Liotta, F., Cosmi, L. & Annunziato, F. Biological and clinical significance of T helper 17 cell plasticity. *Immunology* 158, 287–295 (2019).
45. Lee, W. & Suresh, M. Vaccine adjuvants to engage the cross-presentation pathway. *Front. Immunol.* 13, 940047 (2022).
46. Rivera, F. & Espino, A. M. Adjuvant-enhanced antibody and cellular responses to inclusion bodies expressing FhSAP2 correlates with protection of mice to *Fasciola hepatica*. *Exp Parasitol* 160, 31–38 (2016).
47. Sachdev, D., Gough, K. & Flynn, RJ. The Chronic Stages of Bovine *Fasciola hepatica* Are Dominated by CD4 T-Cell Exhaustion. *Front. Immunol.* 8, (2017).
48. Harris, D. P. *et al.* Reciprocal regulation of polarized cytokine production by effector B and T cells. *Nat Immunol* 1, 475–482 (2000).

49. Mo, C. *et al.* SARS-CoV-2 mRNA vaccine requires signal peptide to induce antibody responses. *Vaccine* 41, 6863–6869 (2023).
50. Pleasance, J., Wiedosari, E., Raadsma, H. W., Meeusen, E. & Piedrafita, D. Resistance to liver fluke infection in the natural sheep host is correlated with a type-1 cytokine response. *Parasite Immunol* 33, 495–505 (2011).
51. Cwiklinski, K. & Dalton, J. P. Exploiting comparative omics to understand the pathogenic and virulence-associated protease: Anti-protease relationships in the zoonotic parasites *Fasciola hepatica* and fasciola gigantica. *Genes* 13, (2022).
52. Maggioli, G. *et al.* The recombinant gut-associated M17 leucine aminopeptidase in combination with different adjuvants confers a high level of protection against *Fasciola hepatica* infection in sheep. *Vaccine* 29, 9057–9063 (2011).

Figures

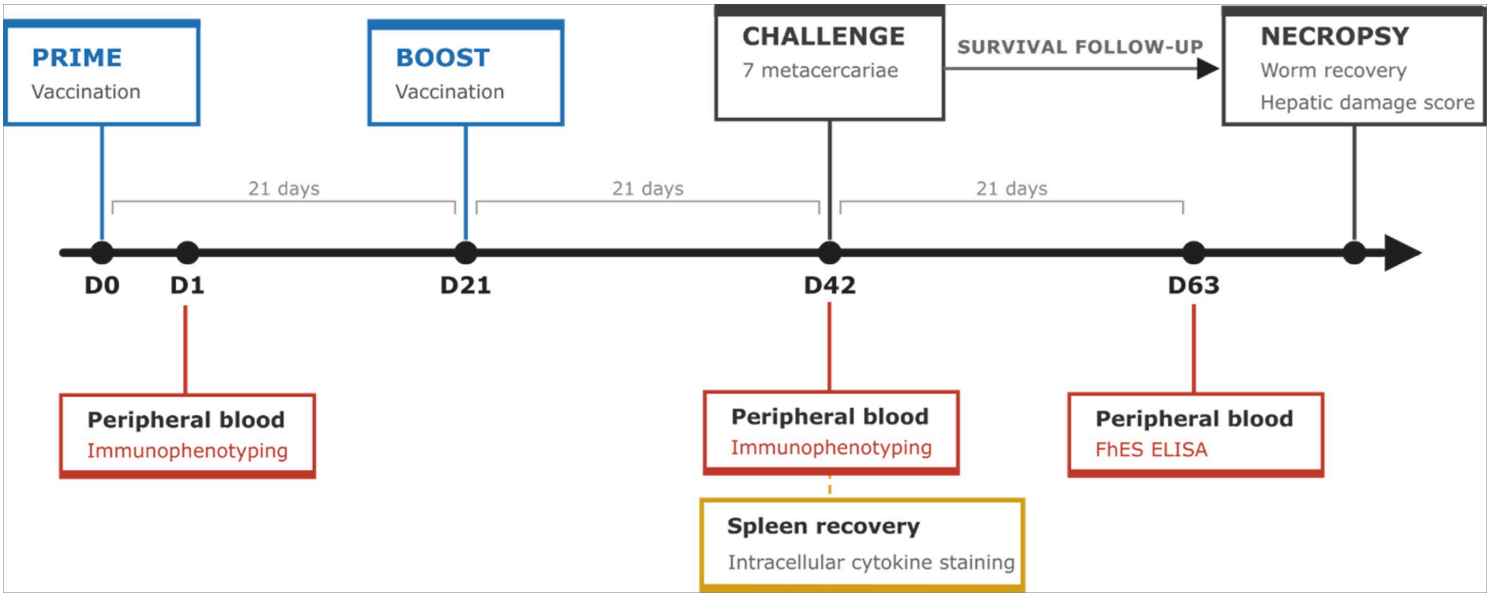


Figure 1

Schematic overview of the vaccination, challenge, and sampling schedule used in this study. Mice were divided into 4 groups: Untreated (n=9), Infection (n=6), eGFP (n=9), and eGFP-Fh3Tq (n=9), and received a prime-boost vaccination regimen 21 days apart. Peripheral blood was sampled on D1, D42, and D63. 3 mice per group in untreated, eGFP, and eGFP-Fh3Tq were sacrificed for intracellular cytokine staining of splenocytes on D42. The remaining 6 mice per group were orally challenged with 7 *Fasciola hepatica*metacercariae (except for the untreated group). All mice underwent necropsy to recover worms and score liver lesions.

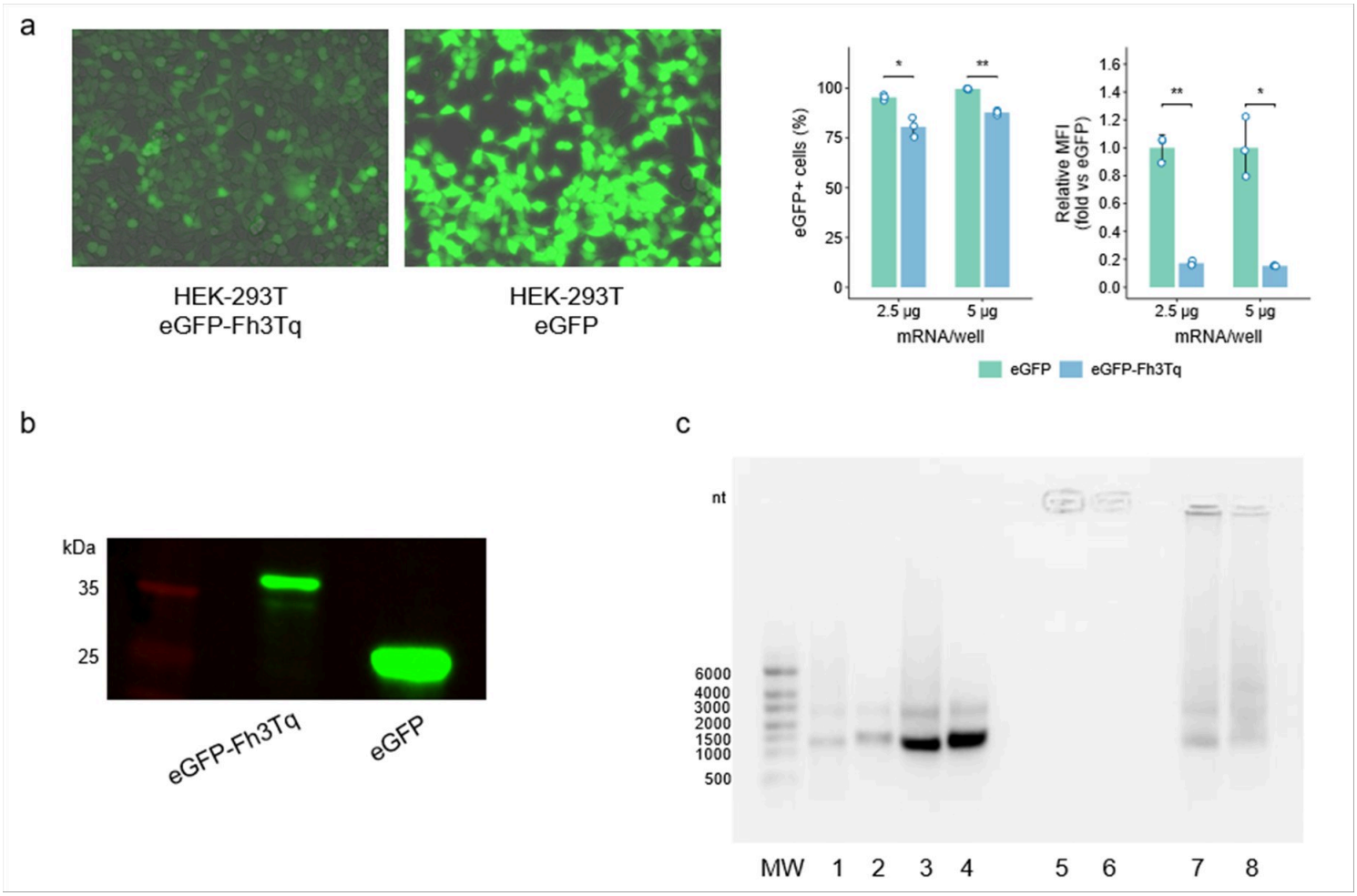


Figure 2

***In vitro* expression and SLN vector characterization of mRNA constructs.**(a) Fluorescence microscopy of HEK293T cells transfected with eGFP-Fh3Tq or eGFP mRNA (5 µg mRNA/well, 24-well plates) using Lipofectamine MessengerMAX, left plot shows flow cytometry quantification of eGFP⁺ cells (%); right plot shows relative median fluorescence intensity (MFI, fold compared to eGFP) at 2.5 and 5 µg/well. Bars represent mean ± SD, differences by paired t-test comparison. (b) Western blot of HEK293T lysates (5 µg mRNA/well) probed with anti-His tag antibody (c). Agarose gel electrophoresis assessing mRNA binding, protection, and release capacity of SLN-based vectors. 1. Free eGFP mRNA, 2. Free eGFP-Fh3Tq mRNA, 3. Free eGFP mRNA + SDS, 4. Free eGFP-Fh3Tq mRNA + SDS, 5. eGFP mRNA-SLN binding, 6. eGFP-Fh3Tq mRNA-SLN binding, 7. eGFP mRNA-SLN release, 8. eGFP-Fh3Tq mRNA-SLN release

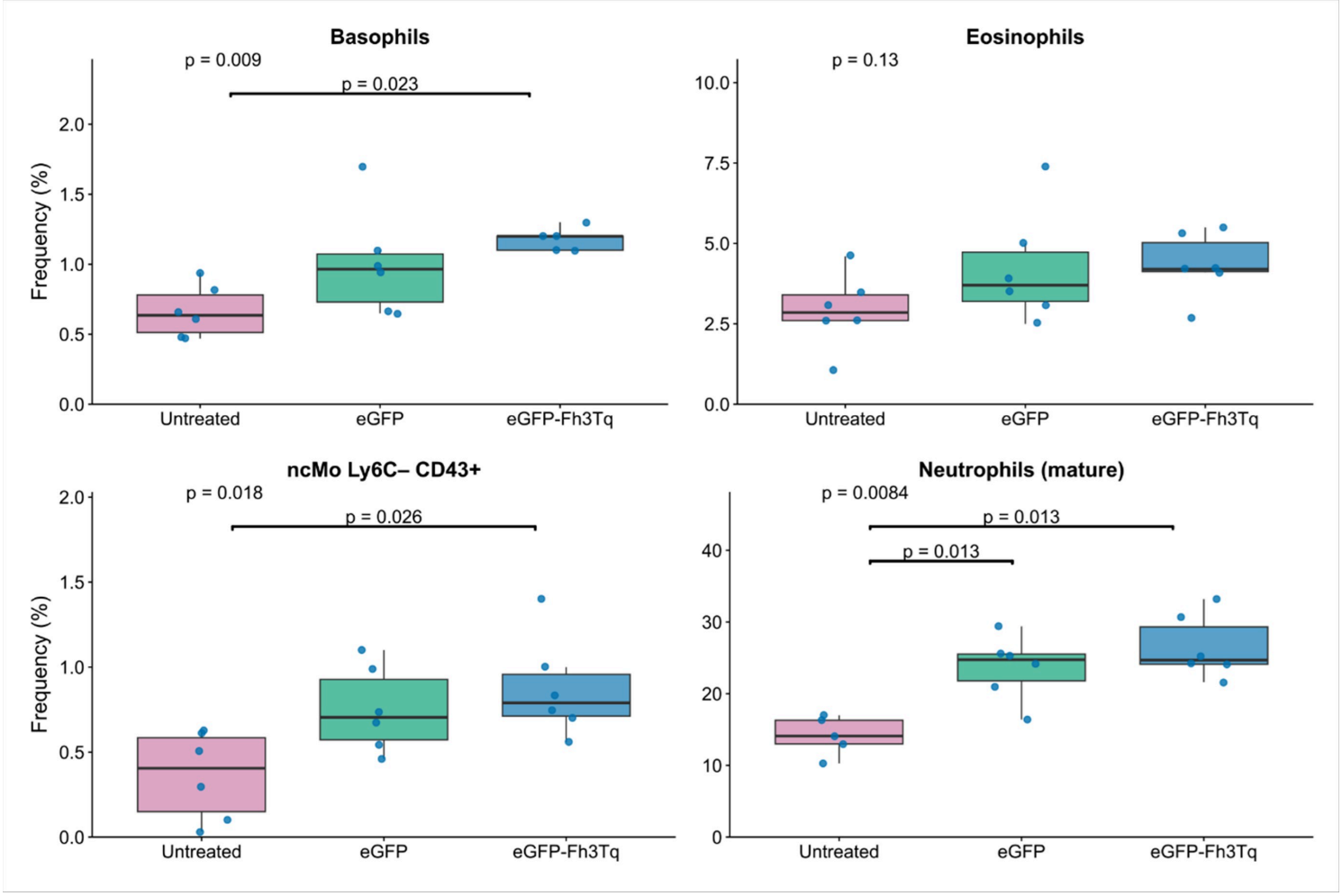


Figure 3

Modulation of innate immune cell populations following SLN-mRNA vaccination. Frequency from live leukocytes (%) of basophils, eosinophils, non-classical monocytes, and mature neutrophils in peripheral blood 24 hours after vaccination, assessed by flow cytometry. Boxplots display the median and interquartile range, along with individual data points. Groups: Untreated (PBS control), eGFP (SLN-eGFP mRNA), and eGFP-Fh3Tq (SLN-eGFP-Fh3Tq mRNA). Significant differences were determined using the Kruskal-Wallis test followed by the pairwise Wilcoxon rank-sum test with Benjamini-Hochberg correction; adjusted p-values are shown.

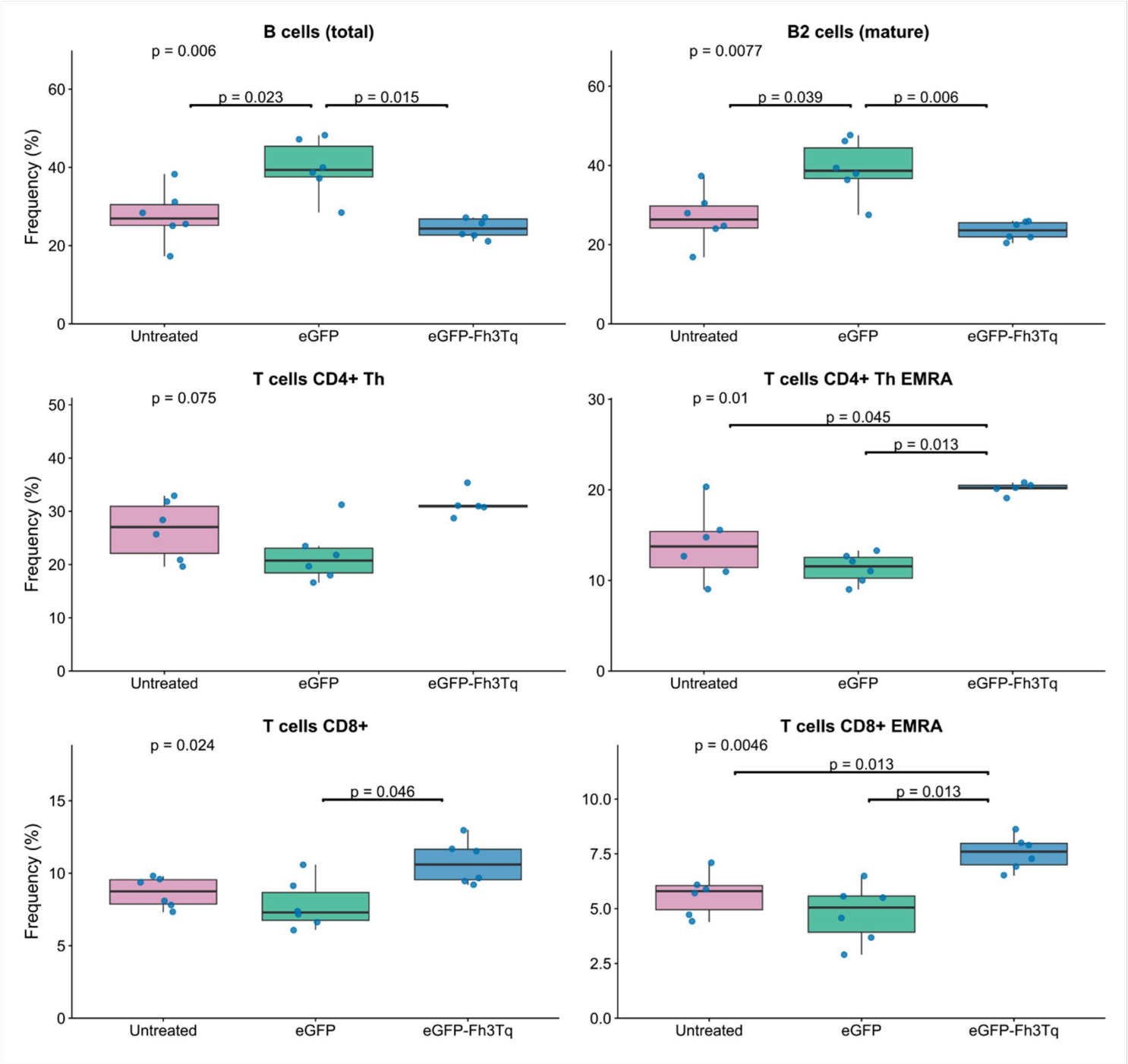


Figure 4

Modulation of adaptive immune cell populations following SLN-mRNA vaccination. Frequency (%) of total B cells, mature B2 cells, total and EMRA CD4$^+$ Th cells, and total and EMRA CD8$^+$ T cells, in peripheral blood at day 42 post-vaccination, assessed by flow cytometry. Boxplots display the median and interquartile range, along with individual data points. Groups: Untreated (PBS control), eGFP (SLN-eGFP mRNA), and eGFP-Fh3Tq (SLN-eGFP-Fh3Tq mRNA). Significant differences were determined using the Kruskal-Wallis test followed by the pairwise Wilcoxon rank-sum test with Benjamini-Hochberg correction; adjusted p-values are shown.

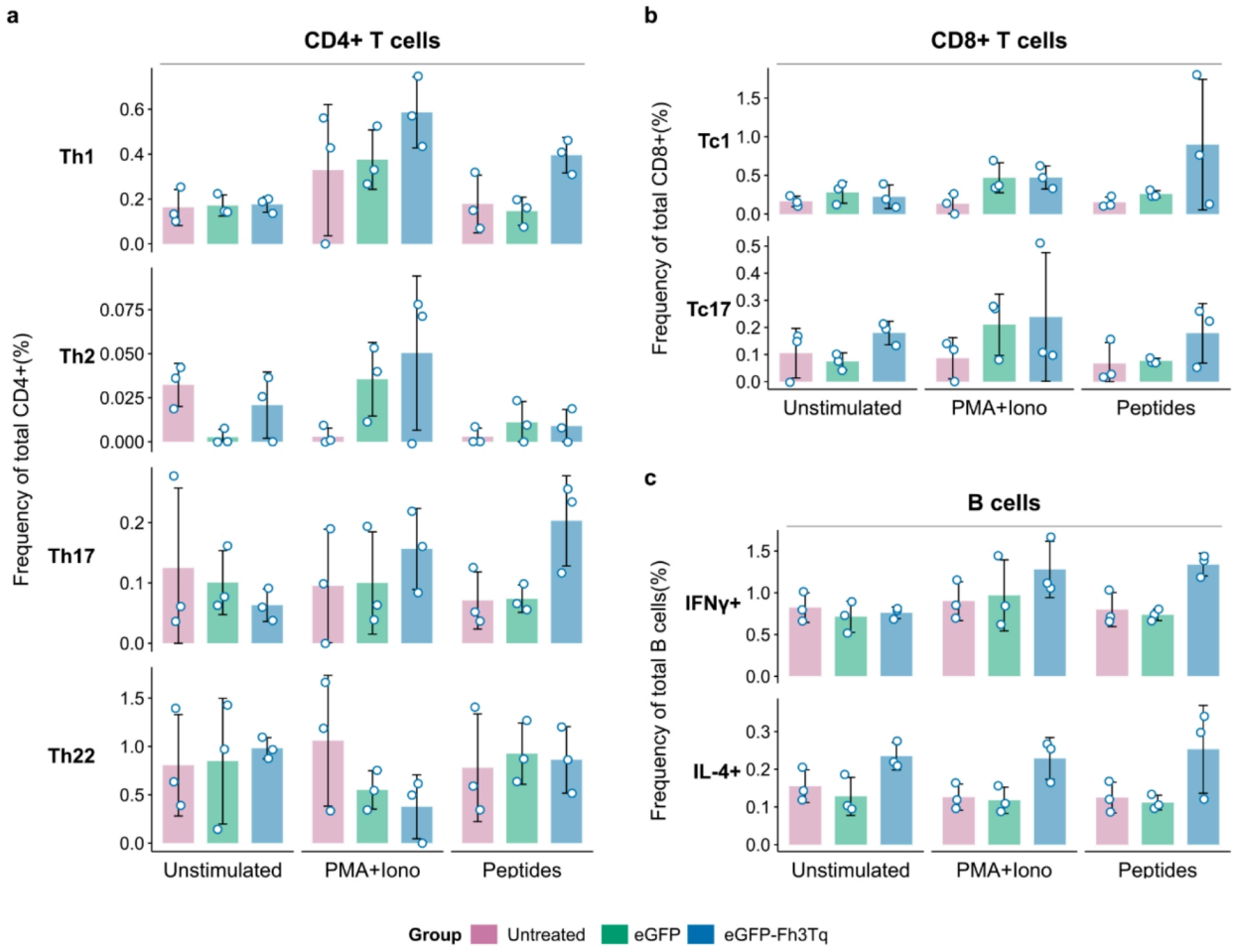


Figure 5

Frequency of cytokine-producing splenocytes from vaccinated mice. Splenocytes collected 42 days post-vaccination were stimulated *ex vivo* with PMA/ionomycin, a pool of T14, T15, T16 peptides, or left unstimulated. Frequencies (expressed as a percentage of the parent population) are shown for (a) Th1, Th2, Th17, and Th22 $CD4^+$ T cells, (b) Tc1 and Tc17 $CD8^+$ T cells, and (c) $IFN\gamma^+$, $IL\text{-}4^+$ cells. Bars represent the mean ± standard deviation, with individual data points (n = 3 per group). The experimental groups are: Untreated (PBS control), eGFP (SLN-eGFP mRNA), and eGFP-Fh3Tq (SLN-eGFP-Fh3Tq mRNA).

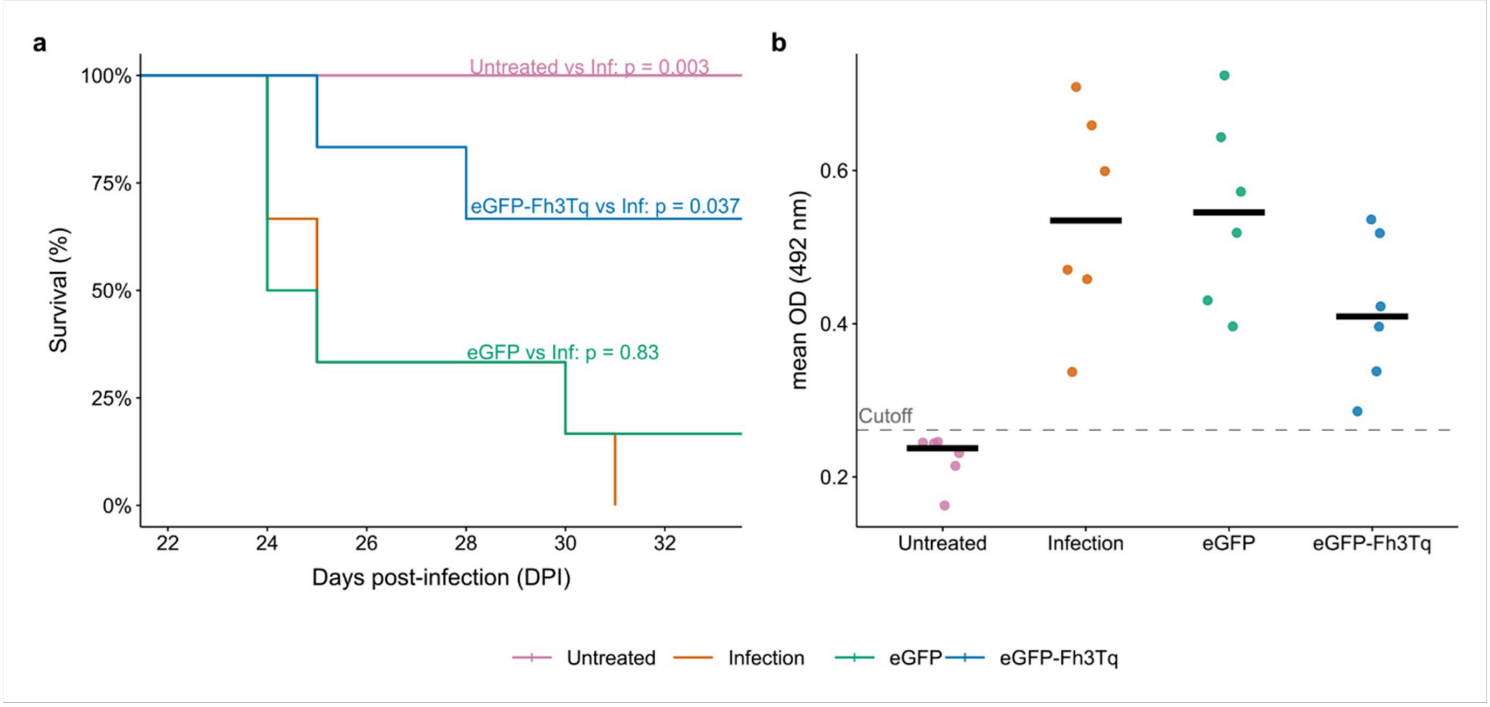


Figure 6

Survival follow-up after *Fasciola hepatica* challenge. a. Kaplan-Meier survival curves of mice challenged with 7 metacercariae. Significant differences were determined using the Log rank test with Benjamini-Hochberg correction; adjusted p-values of pairwise comparisons against the infection group are shown. b. Anti-*F. hepatica* excretory-secretory (FhES) IgG ELISA on pre-necropsy serum. Individual OD values are shown with group means (black bars); the dashed line indicates the positivity cutoff as median + 3MAD.Groups: Untreated (PBS, unchallenged), Infection (PBS, challenged), eGFP (SLN-eGFP mRNA, challenged), and eGFP-Fh3Tq (SLN-eGFP-Fh3Tq mRNA, challenged).

Supplementary Files

This is a list of supplementary files associated with this preprint. Click to download.

- Supplementarymaterial.docx